Direct Conversion of α-Substituted Ketones to Metallo-1,2-enedithiolates

John K. Hsu, Cecilia J. Bonangelino, Sharada P. Kaiwar, Christine M. Boggs, James C. Fettinger, and Robert S. Pilato*

Department of Chemistry and Biochemistry, The University of Maryland, College Park, Maryland 20742

Received February 26, 1996[⊗]

A new synthetic route to metallo-1,2-enedithiolates is presented. The addition of 1 equiv of the α-bromo ketones Ar-C(O)CHXR (X = Br) {Ar = 2-quinoxaline, 2-, 3-, or 4-pyridine, Ph, Cl−Ph, and pyrene (R = H); Ar = 2-quinoxaline (R = Me); and Ar = R = Ph} to $Cp_2Mo(SH)_2$ followed by the addition of base results in the formation of the corresponding metallo-1,2-enedithiolate $Cp_2Mo\{\eta^2\text{-}SC(Ar)C(R)S\}$. The α-tosyl ketones quinoxaline−C(O)CHR−tosyl {R = H, Me} and the α-phosphorylated ketone 3-pyridine-$C(O)CH_2$−O−$P(O)(OEt)_2$ yield the same products as the corresponding α-bromo ketones upon reaction with $Cp_2Mo(SH)_2$. The addition of acid to the heterocyclic substituted complexes yields $Cp_2Mo\{\eta^2\text{-}SC(HetH^+)C(R)S\}$. Both $Cp_2Mo\{\eta^2\text{-}SC(quinoxaline)C(H)S\}$and $[Cp_2Mo\{\eta^2\text{-}SC(quinoxalinium)C(H)S\}][BF_4]$ have been crystallographically characterized. $Cp_2Mo\{\eta^2\text{-}SC(quinoxaline)C(H)S\}$ crystalizes in the *C*2/*c* space group with $a = 21.451(2)$ Å, $b = 15.474$ Å, $c = 12.2201(13)$ Å, and $\beta = 107.440(7)°$. $[Cp_2Mo\{\eta^2\text{-}SC(quinoxalinium)C(H)S\}][BF_4]$ crystalizes in the $P\bar{1}$ space group with $a = 7.4009(8)$ Å, $b = 10.1192(13)°$ Å, $c = 15.930(4)$ Å; $\alpha = 81.49(2)°$, $\beta = 76.14(2)°$, and $\gamma = 85.784°$. In the solid state $[Cp_2Mo\{\eta^2\text{-}SC(quinoxalinium)C(H)S\}][BF_4]$ π-stacks the heterocycle of two adjacent molecules with atom−atom distances of ≈ 3.6 Å. The stacks are limited to pairs of molecules, and there is no long-range order. The pK_a values for the quinoxalinium (R = H and Me) and the 2-, 3-, and 4-pyridinium (R = H) complexes have been determined in acetonitrile to be 1−3 units larger than the free heterocycles. The pK_a of the pyridinium complexes follows the substitution trend 2 ≈ 4 > 3 > free pyridinium and is consistent with resonance stabilization of pyridinium by the metallo-1,2-enedithiolate. Electronic transitions in these complexes have been assigned to a LMCT transition and an ILCT transition by comparison of the various complexes accompanied with solvent sensitivity studies.

Introduction

Considerable research has focused on the synthesis, reactivity, and physical properties of metallo-1,2-enedithiolates.[1−3] These complexes are of interest as components in magnetic[4,5] and conducting[6,7] materials, as solution lumophores,[8−11] and as models for the molybdenum cofactor (Moco).[12−16]

As shown in eq 1, Moco contains a 1,2-enedithiolate at the interface between a molybdenum oxo center (or a tungsten oxo center in the analogous tungsten enzymes) and a pterin (2-amino-4(3*H*)-pteridinone).[17,18] Recent X-ray crystallographic work suggests that at least two Moco enzymes contain a pterin fused pyran.[18,24−26] Rajagopalan and co-workers have isolated the precursor to Moco, a pterin six-substituted with a four carbon side chain.[19−26] The side chain is an α-phosphorylated ketone where the phosphate is contained in a six-membered ring.

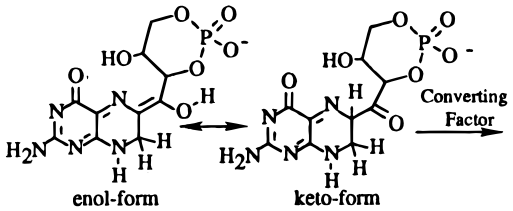

Moco Precursor

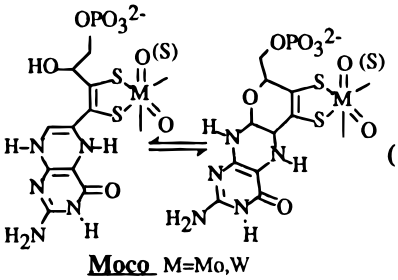

(1)

[⊗] Abstract published in *Advance ACS Abstracts,* July 1, 1996.

(1) Zuleta, J. A.; Burberry, M. S.; Eisenberg, R. *Coord. Chem. Rev.* **1990**, *97*, 47.
(2) Pilato, R. S.; Stiefel, E. I. Catalysis by Molybdenum-Cofactor Enzymes. In *Bioinorganic Catalysis*; Reedijk, J., Ed.; Marcel Dekker Inc.: New York, 1993; pp 133−188.
(3) Cassoux, P.; Valade, L.; Kobayashi, H.; Kobayashi, A.; Clark, R. A.; Underhill, A. E. *Coord. Chem. Rev.* **1991**, *110*, 115.
(4) Manoharan, P. T.; Noordik, J. H.; de Boer, E.; Keijzers, C. P. *J. Chem. Phys.* **1980**, *74*, 1980.
(5) Kuppusamy, P.; Manoharan, P. T. *Chem. Phys. Lett.* **1985**, *118*, 159.
(6) Veldhuizen, Y. S. J.; Veldman, N.; Spek, A. L.; Faulmann, C.; Haasnoot, J. G.; Reedijk, J. *Inorg. Chem* **1995**, *34*, 140.
(7) Fourmigue, M.; Lenoir, C.; Coulon, C.; Guyon, F.; Amaudrut, J. *Inorg. Chem.* **1995**, *34*, 4979.
(8) Cummings, D. S.; Eisenberg, R. *Inorg. Chem.* **1995**, *34*, 3396.
(9) Cummings, D. S.; Eisenberg, R. *Inorg. Chem.* **1995**, *34*, 2007.
(10) Bevilacqua, M. J.; Eisenberg, R. *Inorg. Chem.* **1994**, *33*, 2913.
(11) Kaiwar, S. P.; Vodacek, A.; Fettinger, J. A.; Blough, N. V.; Pilato, R. S. Manuscript in preparation.
(12) Pilato, R. S.; Gea, Y.; Eriksen, K. A.; Greaney, M. A.; Stiefel, E. I.; Goswami, S.; Kilpatrick, L.; Spiro, T. G.; Taylor, E. C.; Rheingold, A. L In *ACS Symposium Series*; Stiefel, E. I.; Coucouvanis, D.; Newton, W. E., Eds.; American Chemical Society: Washington, DC, 1993; Vol. 635; pp 83−97.
(13) Armstrong, E. M.; Austerberry, M. S.; Birks, J. H.; Beddoes, R. L.; Helliwell, M.; Joule, J. A.; Garner, C. D. *Heterocycles* **1993**, *35*, 563.
(14) Soricelli, C. L.; Szalai, V. A.; Burgmayer, S. J. N. *J. Am. Chem. Soc.* **1991**, *113*, 9877.
(15) Das, S. K.; Chaudhury, P. K.; Biswas, D.; Sarkar, S. *J. Am. Chem. Soc.* **1994**, *116*, 9061.
(16) Oku, H.; Ueyama, N.; Nakamura, A.; Kai, Y.; Kanehisa, N. *Chem. Lett.* **1994**, 607.
(17) Rajagopalan, K. V.; Johnson, J. L. *J. Biol. Chem.* **1992**, *267*, 10199.
(18) Chan, M. K.; Mukund, S.; Kletzin, A.; Adams, M. W. W.; Rees, D. C. *Science* **1995**, *267*, 1463.
(19) Johnson, J. L.; Wuebbens, M. M.; Rajagopalan, K. V. *J. Biol. Chem.* **1989**, *264*, 13440.
(20) Wuebbens, M. M.; Rajagopalan, K. V. *J. Biol. Chem* **1993**, *268*, 13493.

S0020-1669(96)00205-4 CCC: $12.00

The biosynthesis of Moco suggests that α-substituted ketones could serve as potential precursors to metallo-1,2-enedithiolates. Moco synthesis also suggests that sensitive functional groups (such as a pterin) should be tolerated in a synthetic route modeled after Moco biosynthesis. A review of the synthetic methods to metallo-1,2-enedithiolates, shown in eqs 2−6,

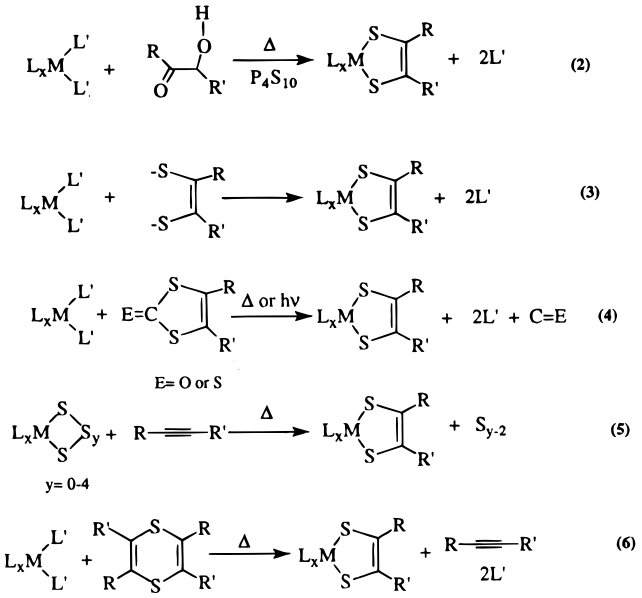

includes a method where an α-hydroxy ketone is the organic precursor. This approach, shown in eq 2, requires the sulfiding agent P_4S_{10} and the generation of a thiophosphate intermediate.[27,28] While this method has allowed a number of complexes to be prepared, it is limited to the synthesis of metallo-1,2-enedithiolates that do not include functional groups that would react with P_4S_{10}, a potent sulfiding agent. With some exceptions,[29,30] most other synthetic methods require electron-withdrawing functional groups either to stabilize the free 1,2-enedithiolate dianion or to activate an alkyne for reaction with a metal polysulfido complex. This accounts for the large number of metal complexes that contain the 1,2-enedithiolate ligands $[S_2C_2R_2]^{2-}$ where R = CN, C(O)Me, C(O)OMe, CF_3, and Ph.[31−38] Pterin substituted metallo-1,2-enedithiolates have been prepared using the method shown in eq 5. The R′ group in these reactions was limited to R′ = −C(O)CH_2R, a group that serves to activate the alkyne.[11,38] In an attempt to develop a new synthetic route to 1,2-enedithiolates, we have drawn from the biological synthesis of Moco and have studied the direct conversion of α-substituted ketones to metallo-1,2-enedithiolates. This paper reports the novel synthesis of new metallo-1,2-enedithiolates from the reaction of the bis(hydrosulfido) complex, $Cp_2Mo(SH)_2$, with α-bromo, α-tosyl, and α-phosphorylated ketones. The Cp_2Mo framework was selected for this initial study since its metallo-1,2-enedithiolates are known to be stable and easily isolated.[7,38,39] Also included in this paper are spectroscopic studies that have defined the electronic transitions in a number of heterocyclic substituted 1,2-enedithiolates and pK_a studies that help to define the effects of the 1,2-enedithiolate on an appended heterocycle.

Experimental Section

Materials. $Cp_2Mo(SH)_2$,[39] (bromoacetyl)-2-quinoxaline,[40] 1-(quinoxalin-2-yl)-2-bromopropanone,[40] (bromoacetyl)-2-pyridine,[41] (bromoacetyl)-3-pyridine,[41] and (bromoacetyl)-4-pyridine[41] were prepared according to the literature procedures. (Tosylacetyl)-2-quinoxaline and 1-(quinoxalin-2-yl)-2-tosylethanone were prepared from the reaction of the bromides with Ag(tosylate) in refluxing acetonitrile.[42] Pyridinium tetraphenylborate was isolated as the precipitate from the reaction of pyridinium chloride and sodium tetraphenylborate in H_2O. Densyl bromide, 2-bromoacetophenone, 2-bromo-4-chloroacetophenone, 1-(bromoacetyl)pyrene, ethyldiisopropylamine, HBF_4−etherate, pyridine, and Ag(tosylate) were purchased from Aldrich and used without further purification. All reactions were performed under an atmosphere of nitrogen using standard Schlenk line techniques. Workups were preformed in air unless stated otherwise. Dichloromethane, acetonitrile, and pentane were dried over calcium hydride and distilled under nitrogen. Diethyl ether, tetrahydrofuran, and dioxane were dried over sodium/benzophenone and distilled under nitrogen. Triethylamine was dried over potassium hydroxide and vacuum distilled.

Physical Measurements. NMR measurements were made on either a Brüker AF 200 or a Brüker AM 400. ESR measurments were made on a Brüker ES-D 200. IR spectra were collected on either a Perkin-Elmer 1600 Series FT-IR spectrometer or a Nicolet 5 DXL FT-IR spectrometer. Mass spectral data were collected on a Magnetic Sector VG 7070E. Chemical analyses were preformed by M-H-W Laboratories.

Synthetic Procedures. Preparation of $Cp_2Mo\{\eta^2$-SC(2-quinoxaline)C(H)S$\}$ (7). To a dichloromethane solution of $Cp_2Mo(SH)_2$ (0.100 g, 0.342 mmol) was added (bromoacetyl)-2-quinoxaline (0.086 g, 0.342 mmol). To this blue solution was added ethyldiisopropylamine, dropwise, until it became deep red. The red solution was evaporated to dryness in air. The solid was chromatographed in air on a 2.5 cm × 20 cm silica gel (60−200) column, and the product was eluted with 2% methanol:dichloromethane. This solution was evaporated to dryness to give **7** as a red solid in 53% yield (0.081 g, 0.182 mmol). Crystallization from dichloromethane−pentane gave analytically pure

(21) Pitterle, D. M.; Rajagopalan, K. V. *J. Biol. Chem.* **1993**, *268*, 13499.
(22) Pitterle, D. M.; Johnson, J. L.; Rajagopalan, K. V. *J. Biol.Chem.***1993**, *268*, 13506.
(23) Pitterle, D. M.; Rajagopalan, K. V. *J. Bacteriol.* **1989**, *171*, 3373.
(24) Romao, M. J.; Archer, M.; Moura, I.; Moura, J. J. G.; LeGall, J.; Engh, R.; Schneider, M.; Hof, P.; Huber, R. *Science* **1995**, *270*, 1170.
(25) Albert, A.; Mizuno, H. *J. Chem. Soc. B* **1971**, 2423.
(26) Albert, A.; Mizuno, H. *J. Chem. Soc., Perkin Trans.* **1973**, 1615.
(27) Schrauzer, G. N.; Mayweg, V. P.; Heinrich, W. *Inorg. Chem.* **1965**, *4*, 1615.
(28) Graczyk, A.; Bialkowska, E.; Konarzewski, A. *Tetrahedron* **1982**, *38*, 2715.
(29) Garner, C. D.; Armstrong, E. M.; Ashcroft, M. J.; Austerberry, M. S.; Birks, J. H.; Collision, D.; Goodwin, A. J.; Larsen, L.; Rowe, D. J.; Russell, J. R. In *Molybdenum Enzymes, Cofactor, and Model Systems*; Stiefel, I. E.; Coucouvanis, D.; Newton, E. W. Eds.; ACS Symposium Series 535, American Chemical Society: Washington, DC, 1993; pp 98−113.
(30) Rakowski DuBois, M.; Haltiwanger, R. C.; Miller, D. J.; Glatzmaier, G. *J. Am. Chem. Soc.* **1979**, *101*, 5245.
(31) Churchill, M. R.; Fennessey, J. P. *Inorg. Chem.* **1968**, *7*, 1123.
(32) Kusters, W.; de Mayo, P. *J. Am. Chem. Soc.* **1974**, *96*, 3502.
(33) Bolinger, C. M.; Rauchfuss, T. B. *Inorg. Chem.* **1982**, *21*, 3947.
(34) Boyde, S.; Garner, C. D.; Joule, J. A.; Rowe, D. J. *J. Chem. Soc.; Chem. Commun.* **1987**, 800.
(35) King, R. B.; Bisnette, M. B. *Inorg. Chem* **1967**, *6*, 469.
(36) Stiefel, E. I.; Bennett, Z. D.; Crawford, T. H.; Simo, C.; Gray, H. B. *Inorg. Chem.* **1970**, *9*, 281.
(37) Yoshinaga, N.; Ueyama, N.; Okamura, T.; Nakamura, A. *Chem. Lett.* **1990**, 1655.
(38) Pilato, R. S.; Eriksen, K. A.; Greaney, M. A.; Stiefel, E. I.; Goswami, S.; Kilpatrick, L.; Spiro, T. G.; Taylor, E. C.; Rheingold, A. L. *J. Am. Chem. Soc.* **1991**, *113*, 9372.
(39) Green, M. L. H.; Lindsell, W. E. *J. Chem. Soc A* **1967**, 1455.
(40) Rowe, D. J.; Garner, C. D.; Joule, J. A. *J. Chem. Soc., Perkin Trans. 1* **1985**, 1907.
(41) Menasse, R. v.; Klein, G.; Erlenmeyer, H. *Helv. Chim. Acta* **1955**, *38*, 1289.
(42) Unpublished results. **Tosylacetyl-2-quinoxaline.** ^{1}H NMR ($CDCl_3$): δ 9.43 (s, 1H, $C_8H_5N_2$), 8.3−8.0 (m, 2H, $C_8H_5N_2$), 7.9 (m, 2H, $C_8H_5N_2$) 7.76 (d, 2 H, C_6H_4 J_{H-H} = 8 Hz) 7.24 (d, 2 H, C_6H_4 J_{H-H} = 8 Hz), 5.75 (s, 2H, CH_2), 2.44 (s, 2H, CH_3). Mass spectrum (EI): m/z = 342 (M^+) **1-(Quinoxalin-2-yl)-2-tosylethanone.** ^{1}H NMR ($CDCl_3$): δ 9.37 (s, 1H, $C_8H_5N_2$), 8.3−8.0 (m, 2H, $C_8H_5N_2$), 7.9 (m, 2H, $C_8H_5N_2$) 7.76 (d, 2 H, C_6H_4 J_{H-H} = 8 Hz) 7.24 (d, 2 H, C_6H_4 J_{H-H} = 8 Hz), 6.50 (q, 1H, C*H*Me, J_{H-H} = 7 Hz) 2.33 (s, 2H, CH_3), 1.62 (d, 3H, CH_3, J_{H-H} = 7 Hz). Mass spectrum (EI): m/z = 357 (M^+).

material. Anal. Calcd for $C_{20}H_{16}MoN_2S_2$: C, 54.05; H, 3.63; N, 6.30. Found: C, 54.13; H, 3.64; N, 6.14. ^{1}H NMR ($CDCl_3$): δ 9.21 (s, 1H, $C_8H_5N_2$), 8.18−8.08 (m, 2H, $C_8H_5N_2$), 7.92−7.80 (m, 1H, C_8H_5 N_2), 7.77 (s, 1H, C_2H), 7.60−7.48 (m, 1H, $C_8H_5N_2$), 5.29 (s, 10H, C_5H_5). UV−vis [abs] (CH_2Cl_2): λ_{max} (ϵ) = 320 (10 900), 492 nm (5280). IR (KBr): 3109 (w), 3050 (w), 1540 (s), 1505 (vs), 1481 (s), 1365 (m), 1309 (m), 1205 (m), 1131 (m), 1016 (m), 996 (m), 903 (m), 838 (s), 812 (s), 763 (s) cm^{-1}. Mass spectrum (EI) m/z = 446 (M^+).

Preparation of $Cp_2Mo\{\eta^2$-S(2-quinoxaline)C(Me)S$\}$ (8). This was prepared as described for **7** using 1-(quinoxalin-2-yl)-2-bromopropanone (0.122 g, 0.342 mmol) in place of bromoacetyl-2-quinoxaline. Complex **8** was isolated as a red solid in 49% yield (0.077 g, 0.168 mmol) Anal. Calcd for $C_{21}H_{18}MoN_2S_2$: C, 55.03; H, 4.96; N, 6.11. Found: C, 54.89; H, 4.62; N, 6.36. ^{1}H NMR ($CDCl_3$): δ 9.05 (s, 1H, $C_8H_5N_2$), 8.05−7.95 (m, 2H, $C_8H_5N_2$), 7.65−7.59 (m, 2H, C_8H_5 N_2), 5.29 (s, 10H, C_5H_5), 2.35 (s, 3H, CH_3). UV−vis [abs] (CH_2Cl_2) λ_{max} (ϵ) = 321-(14 900), 518 (3770). IR (KBr): 3110 (w), 3050 (w), 2890 (w), 2910 (w), 2960 (w), 1565 (m), 1528 (s), 1435 (m), 1365 (m), 1332 (m), 1267 (m), 1203 (s), 1135 (m), 1015 (m), 999 (m), 955 (m), 936 (m), 834 (s), 815 (s), 763 (s), 738 (m), 562 (m), 413 (m) cm^{-1}. Mass spectrum (EI): m/z = 460 (M^+), 228 (M^+ − quinoxalin−(methyl)−1,2-enedithiolate).

Preparation of $Cp_2Mo\{\eta^2$-SC(2-pyridine)C(H)S$\}$ (9). To an acetonitrile solution of $Cp_2Mo(SH)_2$ (0.100 g, 0.342 mmol) was added (bromoacetyl)-2-pyridine (0.068 g, 0.342 mmol). The mixture was allowed to stir for 20 min and became a deep red. To the solution was added ethyldiisopropylamine, dropwise, until the solution become brown. The brown solution was evaporated to dryness in air. The solid was chromatographed in air on a 2.5 cm × 20 cm silica gel (60−200) column and was eluted with 2% methanol−dichloromethane. This solution was evaporated to dryness to give **9** as a brown solid in 29% yield (0.039 g, 0.099 mmol). Anal. Calcd for $C_{17}H_{15}MoNS_2$: C, 51.91; H, 3.84; N, 3.56. Found: C, 51.91; H, 3.90; N 3.38. ^{1}H NMR ($CDCl_3$): δ 8.48 (m, 1H, C_6H_4N), 7.68 (m, 1H, C_6H_4N), 7.65 (m, 1H, C_6H_4N), 7.39 (s, 1H, C_2H), 6.92 (m, 1H, C_6H_4N), 5.28 (s, 10H, $2C_5H_5$). UV−vis [abs] [CH_2Cl_2]: λ_{max} (ϵ) = 380 (5750), 548 (1460). IR (KBr): 3107 (w), 1614 (m), 1581 (s), 1519 (m), 1491 (m), 1460 (m), 1439 (m), 1424 (m), 1128 (m), 1021 (m), 1001 (m), 921 (m), 837 (s), 818 (m), 759 (m) cm^{-1}. Mass spectrum (EI): m/z = 395 (M^+).

Preparation of $Cp_2Mo\{\eta^2$-SC(3-pyridine)C(H)S$\}$ (10). This was prepared as described for **9** with (bromoacetyl)-3-pyridine (0.068 g, 0.342 mmol) in place of (bromoacetyl)-2-pyridine. Complex **9** was isolated as a brown solid in 27% yield (0.036 g, 0.092 mmol). Anal. Calcd for $C_{17}H_{15}MoNS_2$: C, 51.91; H, 3.84; N, 3.56. Found: C, 52.44; H, 4.33; N, 3.54. ^{1}H NMR ($CDCl_3$): δ 8.86 (s, 1H, C_6H_4N), 8.28 (d, [J_{H-H} = 5 Hz], 1H, C_6H_4N), 7.90 (d, [J_{H-H} = 8 Hz], 1H, C_6H_4N), 7.12 (dd, [J_{H-H} = 5 Hz] [J_{H-H} = 8 Hz], 1H, C_6H_4N), 6.85 (s, 1H, C_2H), 5.27 (s, 10H, $2C_5H_5$). UV−vis [abs] (CH_2Cl_2): λ_{max} (ϵ) = 371 (5540), 547 (1460). IR (KBr): 3092 (w), 3050 (w), 2970 (w), 1581 (m), 1532 (s), 1475 (s), 1439 (s), 1404 (s), 1233 (m), 1124 (m), 1021 (s), 1005 (s), 907 (m), 828 (vs), 817 (vs), 801 (vs), 765 (vs), 711 (s), 660 (m), 605 (s), 586 (m), 551 (s), 450 (w), 313 (m), 365 (m) cm^{-1}. Mass spectrum (EI): m/z = 395 (M^+).

Preparation of $Cp_2Mo\{\eta^2$-SC(4-pyridine)C(H)S$\}$ (11). This was prepared as described for **9** with (bromoacetyl)-4-pyridine (0.068 g, 0.342 mmol) in place of (bromoacetyl)-2-pyridine. Complex **11** was isolated as a brown solid in 23% yield (0.031 g, 0.079 mmol). Anal. Calcd for $C_{17}H_{15}MoNS_2$: C, 51.91; H, 3.84. Found: C, 52.20; H, 3.46. ^{1}H NMR ($CDCl_3$): δ 8.36(d, [J_{H-H} = 6 Hz], 2H, C_6H_4N), 7.50 (d, [J_{H-H} = 6 Hz], 2H, C_6H_4N), 7.14 (s, 1H, C_2H), 5.27 (s, 10H, $2C_5H_5$). UV−vis [abs] (CH_2Cl_2): λ_{max} (ϵ) = 382 (5350), 537 (1520). IR (KBr): 3119 (w), 3091 (w), 3037 (w), 1597 (s), 1586 (vs), 1541 (vs), 1515 (vs), 1409 (s), 1211 (s), 989 (vs), 919 (s), 833 (s), 813 (s), 804 (s), 772 (vs), 731 (s), 671 (m), 652 (s), 608 (s), 555 (m), 458 (m), 393 (m). Mass spectrum (EI) m/z = 395 (M^+).

Preparation of $Cp_2Mo\{\eta^2$-SC(phenyl)C(phenyl)S$\}$ (12). This was prepared as described for **7** with densyl bromide (0.068 g, 0.342 mmol) in place of (bromoacetyl)-2-quinoxaline. Complex **12** was isolated in 40% yield as a brown solid (0.054 g, 0.137 mmol). Anal. Calcd for $C_{24}H_{20}MoS_2$: C, 61.53; H, 4.30. Found: C, 61.11; H, 4.61. ^{1}H NMR ($CDCl_3$): δ 7.18−6.95 (m, 10H, $2C_6H_5$) 5.29 (s, 10H, $2C_5H_5$). UV−vis [abs] (CH_2Cl_2): λ_{max} (ϵ) = 371 (5030), 570 (1940). IR (KBr): 3116 (w), 3077 (w), 3026 (w), 3056 (w), 1595 (s), 1574 (m), 1560 (m), 1490 (m), 1479 (m), 1437 (m), 1243 (m), 1065 (m), 1026 (m), 1016 (m), 1002 (m), 913 (m), 903 (m), 865 (m), 835 (s), 825 (s), 810 (s), 758 (s), 737 (vs), 704 (s), 691 (vs), 640 (m), 630 (m), 609 (m), 516 (m), 506 (m) cm^{-1}. Mass spectrum (EI): m/z = 470 (M^+), 228 (M^+ − diphenyl-1,2-enedithiolate).

Preparation of $Cp_2Mo\{\eta^2$-SC(phenyl)C(H)S$\}$ (13). This was prepared as described for **7** with 2-bromoacetophenone (0.061 g, 0.306 mmol) in place of (bromoacetyl)-2-quinoxaline. Complex **13** was isolated as a brown solid in 26% yield (0.032 g, 0.081 mmol). Anal. Calcd for $C_{18}H_{16}MoS_2$: C, 55.10; H, 4.11. Found: C, 54.96; H, 4.48. ^{1}H NMR ($CDCl_3$): δ 7.63 (m, 2H, C_6H_5), 7.25−7.15 (m, 4H, C_6H_5 and C_2H), 5.25 (s, 10H, $2C_5H_5$). UV−vis [abs] (CH_2Cl_2): λ_{max} (ϵ) = 361 (4470), 565 (1310). IR (KBr): 3136 (w), 3067 (w), 3053 (w), 3011 (w), 1589 (s), 1571 (s), 1528 (vs), 1483 (s), 1437 (s), 1420 (s), 1211 (m), 1072 (m), 1017 (m), 1000 (m), 901 (m), 831 (s), 813 (vs), 750 (vs), 692 (s), 654 (m), 604 (m) cm^{-1}. Mass spectrum (EI): m/z = 394 (M^+), 228 (M^+ − phenyl(H)−enedithiolate).

Preparation of $Cp_2Mo\{\eta^2$-SC(*p*-chlorophenyl)C(H)S$\}$ (14). Prepared as described for **7** with (0.095 g, 0.407 mmol) 2-bromo-4-chloroacetophenone in place of (bromoacetyl)-2-quinoxaline. Complex **14** was isolated as a brown solid in 27% yield (0.038 g, 0.089 mmol). Anal. Calcd for $C_{18}H_{15}ClMoS_2$: C, 50.65; H, 3.54. Found: C, 51.01; H, 4.01. ^{1}H NMR ($CDCl_3$): δ 7.56 (d, [J_{H-H} = 8 Hz], 2H, C_6H_4Cl), 7.16 (d, [J_{H-H} = 8 Hz], 1H, C_6H_4Cl), 7.15 (s, 1H,C_2H), 5.26 (s, 10H, $2C_5H_5$). UV−vis [abs] (CH_2Cl_2): λ_{max} (ϵ) = 3369 (6710), 556 (1520). IR (KBr): 3112 (w), 3078 (w), 3054 (w), 3044 (w), 1595 (s), 1477 (m), 1439 (m), 1245 (m), 1065 (m), 1027 (m), 1016 (m), 1000 (m), 836 (s), 825 (s), 811 (s), 757 (m), 738 (vs), 702 (s), 691 (s), 610 (m) cm^{-1}. Mass spectrum (EI): m/z = 428 (M^+), 227 (M^+ − chlorophenylenedithiolate).

Preparation of $Cp_2Mo\{\eta^2$-SC(1-pyrene)C(H)S$\}$ (15). Prepared as described for **7** with 1-(bromoacetyl)pyrene (0.086 g, 0.266 mmol) in place of (bromoacetyl)-2-quinoxaline. Complex **15** was isolated as a brown solid in 51% yield (0.070 g, 0.136 mmol). ^{1}H NMR ($CDCl_3$): 8.45 (d, [J_{H-H} = 10 Hz], 1H, $C_{16}H_9$), 8.11−7.93 (m, 8H, $C_{16}H_9$), 6.50 (s, 1H, C_2H), 5.34 (s, 10H, $2C_5H_5$). UV−vis [abs] (CH_2Cl_2): λ_{max} (ϵ) = 345 (19 500), 351 (20 700), 445 (4120). IR (KBr): 3119 (w), 3104 (w), 3037 (w), 3008 (w), 1596 (m), 1580 (m), 1559 (m), 1542 (m), 1484 (m), 1430 (m), 1420 (m), 1369 (w), 1242 (m), 1180 (m), 1016 (m), 998 (m), 922 (m), 840 (vs), 811 (vs), 761 (s), 718 (vs), 681 (m) cm^{-1}. High resolution mass spectra: calcd for $C_{28}H_{20}{}^{98}MoS_2$, m/z = 518.00604; found, m/z 518.00876.

Structural Determination for $Cp_2Mo\{\eta^2$-SC(2-quinoxaline)-C(H)S$\}\cdot 0.5CH_2Cl_2$ (7). Crystallographic data are collected in Table 1. Crystals were photographically characterized and determined to belong to the monoclinic crystal system. Systematic absences indicated the centrosymmetric space group *C*2/*c* or the noncentrosymmetric space group *Cc*. Intensity statistics clearly indicated the centric case. An absorption correction was applied with transmission factors ranging from 0.8514 to 0.9952, with an average correction of 0.9415. The structure was determined with the successful location of the molybdenum and two sulfur atoms using direct methods. An initial difference map located all remaining non-hydrogen atoms. All hydrogen atoms were directly located from two subsequent difference-Fourier maps. The CH_2Cl_2 solvent molecule's central carbon atom was found to lie at $^1/_2$, *y*, $^1/_4$ and resulted in the location of two half-occupancy chlorine atoms about the local 2-fold axis. Solvent hydrogen atoms were placed in calculated positions that were dependent upon both local geometry restraints and temperature (293 K in this case) with the methylene hydrogen's C−H distance = 0.970 Å and U_H set equal to $1.2U_{parent}$. These calculated positions were optimized after each cycle of the refinement but not refined. The hydrogen atoms on the main molecule were all full occupancy and allowed to refine freely resulting in C−H distances ranging from 0.783 to 1.015 Å and *U*(eq) ranging from 0.041 to 0.072. This clearly supporting refinement of these atoms. All computations used SHELXTL 93 software.[43]

Structural Determination for $[Cp_2Mo\{\eta^2$-SC(2-quinoxalineH)-C(H)S$\}][BF_4]$ (2). Crystallographic data are collected in Table 1.

(43) (a) Gabe, E. J.; Le Page, Y; Charland, J. P.; Lee, F. L.; White, P. S. *J. Appl. Crystallogr.* **1989**, *22*, 384. (b) Sheldrick, G. M. *Acta Crystallogr.* **1990**, *A46*, 467.

Scheme 1

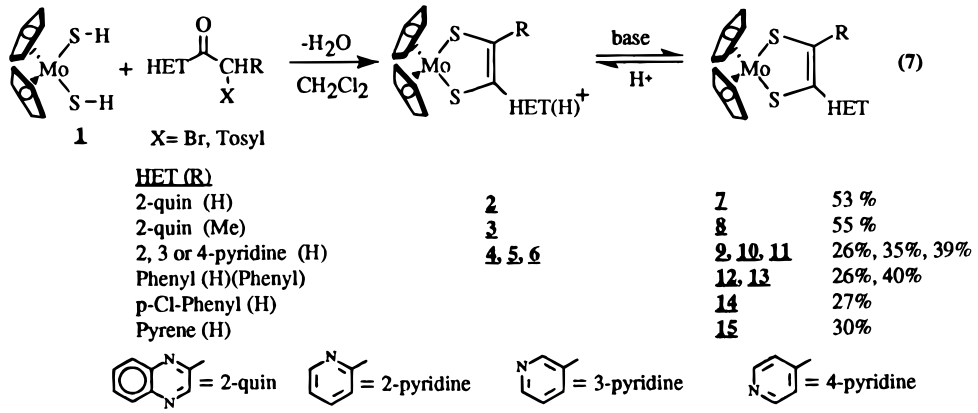

Table 1. Summary of X-ray Crystal Structure Data for Complexes **7** and **2**[a]

	7	**2**
formula	$C_{20.50}H_{17}Cl\ MoN_2S_2$	$C_{21}H_{18}BCl_2\ F_4MoN_2S_2$
fw	486.87	616.14
cryst syst	monoclinic	triclinic
space group:	*C*2/*c*	$P\bar{1}$
a (Å)	21.451(2)	7.4009(8)
b (Å)	15.474(2)	10.1192(13)
c (Å)	12.2201(13)	15.930(4)
α (deg)		81.49(2)
β (deg)	107.440(7)	76.14(2)
γ (deg)		85.784(10)
V (Å^3)	3869.8(7)	1144.6(4)
Z	8	2
ρ_{calc} (g/cm^{-3})	1.671	1.788
T (K)	293(2)	153(2)
radiation, *λ* (Å)	Mo Kα, 0.710 73	Mo Kα, 0.710 73
abs coeff (mm^{-1})	1.039	1.035
wR_2	0.0698	0.1915
R_1	0.0364	0.0764
GOF	1.020	1.113

[a] Residuals $R_1 = \Sigma[|F_o| - |F_c|]/\Sigma|F_o|$ $wR_2 = \{[\Sigma w(F_o^2 - F_c^2)^2]/\Sigma[w(F_o^2)^2]\}^{1/2}$ where $w^{-1} = [\sigma^2(F_o^2) + (0.0422P)^2 + 3.865P]$ for **7** and $w^{-1} = [\sigma^2(F_o^2) + (0.1215P)^2 + 0.49698P]$ for **2** and $P = (\max(F_o^2,0) + 2F_c^2)/3$. GOF $= \delta = [\Sigma[w((F_o^2 - F_c^2)^2]/(n - p)]^{1/2}$ where n = number of reflections and p = number of parameters.

Crystals were photographically characterized and determined to belong to the triclinic crystal system $P\bar{1}$. An absorption correction was applied with transmission factors ranging from 0.586 to 0.997 with an average correction of 0.773. The structure was determined with the successful location of the molybdenum and two sulfur atoms. Subsequent difference-Fourier maps revealed the location of all of the remaining non-hydrogen atoms. Hydrogen atoms were placed in calculated positions that were dependent on both the type of bonding at the central atom and the temperature (153 K in this case) resulting in C−H distances = 0.950 Å, U_H being set equal to $1.2U_{parent}$, and $C-H_2$ distances = 0.990 Å, U_H being set equal to $1.2U_{parent}$. All computations used SHELXTL 93 software.[43]

Electrochemical Experiments. All electrochemical experiments where conducted with a BAS CV50 in either CV or OSW modes using a glassy carbon working, platinum auxiliary, and Ag/AgCl reference electrode with $[NBu_4][PF_6]$ as the supporting electrolyte. The values reported in Table 4 were recorded at 100 mV/s under condition where the ferrocene/ferrocenium couple was found at 452 mV. Complexes **2**−**6** were generated in the electrochemical cell by the addition of either [pyridinium][BPh_4] or HBF_4 etherate to solutions of **7**−**11**. Small samples of the protonated species were removed from the electrochemical cell and diluted and UV−visible spectra recorded to insure that only the monoprotonated species were present. The samples prepared by the addition of HBF_4 and pyridinium were compared by their $\Delta E_{1/2}$ values $\{\Delta E_{1/2} = E_{1/2(protonated)} - E_{1/2(neutral)}\}$.

UV−Visible and pK_a Measurements for Complexes 2−15. All UV−visible experiments were conducted using a Perkin-Elmer (*λ*-2) spectrometer in absorbance mode. Solvent sensitivity plots were generated by graphing absorption λ_{max} vs either E^*_{MLCT} or π^*.[44]

The pK_a measurements for complexes **2**, **3**, and **5** were determined by the progressive addition of [pyridinium][BPh_4] to acetonitrile solutions of **7**, **8**, and **10**, respectively. The concentrations of the metal complexes were determined by single point UV−visible measurements. The pyridinium and pyridine concentrations were determined from the known amount of [pyridinium][BPh_4] added and the relative concentration of the protonated, [**X**H$^+$], and neutral, [**X**], metal complexes. The pK_a values were calculated from the K_{eq} values $\{K_{eq} = [\mathbf{X}H^+][\text{pyridine}]/[\text{pyridinium}][\mathbf{X}] = [\mathbf{X}H^+]^2/([\text{pyridinium}]_{added} - [\mathbf{X}H^+])[\mathbf{X}]$ at five points between 20 and 80% of the initial concentration of the neutral complexes; $pK_a = pK_{a'} + \log K_{eq}$, where $pK_{a'}$ is 12.3 for [pyridinium][BPh_4] in acetonitrile.[45] It was not necessary to consider the formation of [Py−H−Py]$^+$ since its concentration would impart less than a 1% error in the pK_a calculations.[46] The experiments were repeated three times and the results averaged.

The pK_a values for complexes **4** and **6** were determined by the addition of 1 equiv of [pyridinium][BPh_4] to **9** and **11** followed by titration with a standardized solution of pyridine. The pK_a values were calculated at five points from 20 to 80% of the initial concentration of the neutral complexes. The concentrations of the metal complexes were determined from single point UV−visible measurements. The pyridinium and pyridine concentrations were determined from the added amounts and the relative concentration of the protonated and neutral metal complexes. The pK_a values were determined as described above where $K_{eq} = [\mathbf{X}H^+]([\text{pyridine}]_{added} + [\text{pyridinium}]_{added} - [\mathbf{X}])/[\mathbf{X}]^2$. The experiments were repeated three times and the results averaged. The reported uncertainties are the standard deviations of the average pK_a values.

Results and Discussion

Metallo-1,2-enedithiolate Synthesis. The reaction of complex **1** with a range of α-bromo ketones yields the corresponding metallo-1,2-enedithiolate complexes with accompanying loss of H_2O as shown in eq 7, Scheme 1. Complexes **7**−**15** are isolated upon the addition of base and subsequent silica gel column chromatography. Complexes **2**−**6** can be regenerated quantitatively by the addition of a proton source to **7**−**11**, respectively. Both the neutral and protonated complexes are air stable in solution for several days. Replacing the α-bromo ketones Quin−C(O)CHRBr with the α-tosyl ketones Quin−C(O)-CHRTosyl (R = H, Me) did slow the reactions but had no effect on the yield of either complex **7** or **8**, respectively.

As Moco biosynthesis would suggest, the α-phosphorylated ketone **16**[47] is also a viable precursor to a metallo-1,2-enedithiolate. As shown in eq 8, **16** reacts with **1** to yield

(44) Manuta, D. M.; Lees, A. J. *Inorg. Chem.* **1983**, *22*, 3825.
(45) Coetzee, J. F.; Padmanabhan, G. R. *J. Am. Chem. Soc* **1965**, *87*, 5005.
(46) Moore, E. J.; Sullivan, J. M.; Norton, J. R. *J. Am. Chem Soc.* **1986**, *108*, 2257.

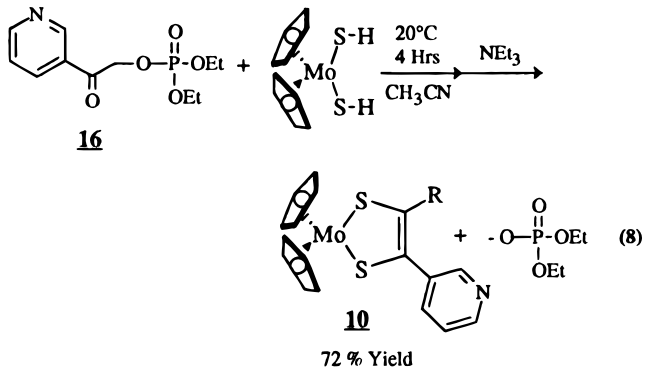

complex **5** with accompanying loss of diethyl phosphate. The addition of triethylamine to the reaction mixture yields complex **10**.

X-ray Crystallographic Results for Complexes 2 and 7. Both complexes **2** (as the BF_4^- salt) and **7** were the subject of single crystal X-ray studies, the results of which are presented in Tables 1 and shown in Figures 1 and 2, respectively. Complex **7** is structurally similar to other molybdenum 1,2-enedithiolate complexes in bond lengths and angles.[36,48,49] The molybdenum 1,2-enedithiolate is a planar five-membered ring. The plane bisects the angle formed by the intersection of the planes of the two cyclopentadienyl ligands. The quinoxaline ring is 26.67°(7) from being coplanar with the five-membered metallo-1,2-enedithiolate. The Mo−S and C−S bonds are best described as single bonds with lengths of 2.4412(14) and 2.4405(12) Å and 1.725(5) and 1.769(5) Å, respectively, and the C(1)−C(2) bond at 1.339(7) Å is best described as a double bond.

Protonation causes substantial changes in the solid state structure of the metallo-1,2-enedithiolate complex as shown in Figure 2. While the 1,2-enedithiolate ligand of **2** is essentially planar {S(1)−C(1)═C(2)−S(2) deviates less than 0.01 Å from the plane}, the molybdenum is 0.344(10) Å out of the plane. The solid state structure of complex **2** is similar to that of $Cp_2Mo^V\{S_2C_2(CN)_2\}$[7] and $Cp_2Ti\{S_2C_2(C(O)Me)_2\}$[31] in that while the 1,2-enedithiolate ligand is planar, the metallo-1,2-enedithiolate is not. This is in contrast with the solid state structure of **7** where the the metallo-1,2-enedithiolate is essentially planar.

While the metallocycle of **2** is no longer planar in the solid state, the quinoxaline ring is approaching coplanarity with the 1,2-enedithiolate ligand as is seen in the S(2)−C(2)−C(3)−N(2) dihedral angle of 1.6(13)°. The coplanarity of the quinoxaline and the 1,2-enedithiolate forces the 1,2-enedithiolate proton at the quinoxaline C(3) proton in a configuration that is similar to eclipsed *cis*-butadiene.

In addition to the coplanarity of the quinoxalinium and 1,2-enedithiolate, in the solid state two adjacent molecules of **2** head to tail π-stack as shown in Figure 3. The head to tail stacking places the electron-deficient protonated pyrazine above the benzenoid ring of the quinoxaline of its stacking partner. Solvent molecules separate the stacking pairs, and the BF_4^- anions are well removed from both the metal and ligands. The plane of one quinoxaline ring is an average distance of 3.4 Å from the atoms within the quinoxaline ring of its partner. The atom−atom distances are an average of 3.6 Å, showing that the stack is only slightly staggered.

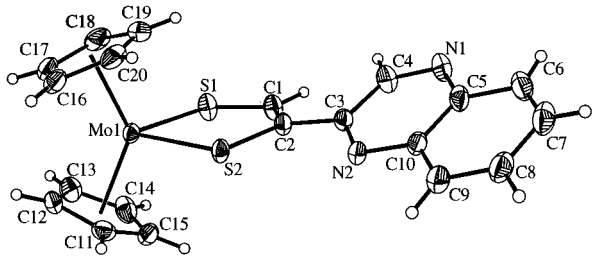

Figure 1. ORTEP drawing of **7** with the thermal ellipsoids drawn at 50% probability. Selected bond lengths (Å) and angles (deg) are as follows: Mo−S(1), 2.4412(14); Mo−S(2), 2.4405(12); S(1)−C(1), 1.725(5); S(2)−C(2), 1.769(5); C(1)−C(2), 1.339(7); C(2)−C(3), 1.463(7); C(3)−C(4), 1.426 (7); C(3)−N(2), 1.315 (7); C(4)−N(1), 1.298(7): S(1)−Mo−S(2), 82.25(4); Mo−S(1)−C(1), 105.68(18); Mo−S(2)−C(2), 106.62(16); S(1)−C(1)−C(2), 125.2(4); S(2)−C(2)−C(1), 119.6 (4); S(2)−C(2)−C(3), 117.7 (4); C(2)−C(3)−N(2); 119.3(4).

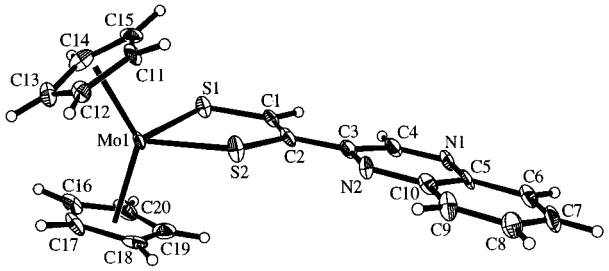

Figure 2. ORTEP drawing of **2** with the thermal ellipsoids drawn at 50% probability. Selected bond lengths (Å) and angles (deg) are as follows: Mo−S(1), 2.458(3); Mo−S(2), 2.437(3); S(1)−C(1), 1.695(11); S(2)−C(2), 1.770(10); C(1)−C(2), 1.33(2); C(2)−C(3), 1.427(14); C(3)−C(4), 1.45(2); C(3)−N(2), 1.336(14); C(4)−N(1), 1.282(14): S(1)−Mo−S(2), 81.30(10); Mo−S(1)−C(1), 106.7(4); Mo−S(2)−C(2), 105.8(3); S(1)−C(1)−C(2), 123.5(8); S(2)−C(2)−C(1), 121.3(8); S(2)−C(2)−C(3), 116.3(4); C(2)−C(3)−N(2); 119.1(9).

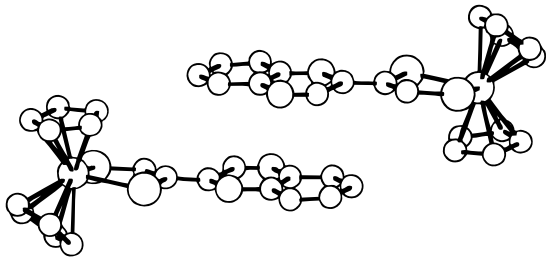

Figure 3. Ball and stick drawing of **2** showing the head to tail π-stacking of the quinoxalinium in the solid state.

Electronic Transitions. The electronic transitions for all of the complexes are shown in Table 2. All of the 1,2-enedithiolate complexes exhibit broad weak ($\epsilon \approx 1500$) absorbance bands at $\approx$550 nm in CH_2Cl_2.

In the quinoxaline complexes this absorbance is overshadowed by a more intense transition ($\epsilon \geq 3700$). However, when the absorbance spectra is taken in nonpolar solvents, such as CCl_4 and toluene, the low intensity band is discernible. This transition is solvent sensitive and shifts to higher energy in more polar solvents. A plot of absorbance energy vs E^*_{MLCT}, a solvent polarity constant for metal charge transfer transitions,[44] as shown for complex **12**, is linear for a broad range of solvents (Figure 4). In alcohols the energy of the absorbance for **12** does not fall on the line with the other solvents. However, as shown, a plot of energy vs E^*_{MLCT} for five alcohols is also linear

(47) Unpublished results. **3-PyC(O)CH$_2$OP(O)(OEt)$_2$ (16).** ^{1}H NMR ($CDCl_3$): δ 9.05 (d, 1H, C_5H_4N, J = 10 Hz), 8.76 (m, 1H, C_5H_4N), 8.15 (m, 1H, C_5H_4N), 7.43 (m, 1H, C_5H_4N), 5.23 (d, 2H,C(O)CH_2, J_{P-H} = 10 Hz), 4.16 (dq, 4H, P−OCH_2CH$_3$, J_{P-H} = 10 Hz, J_{H-H} = 6 Hz), 1.31 (t, 6H, P−OCH$_2$CH_3, J_{H-H} = 6 Hz). ^{13}C NMR ($CDCl_3$): δ 191.6 (d, *C*O, J_{P-C} = 5 Hz), 154, 149.1, 135.2, 129.6, 123.8, 68.6 (d, *C*H$_2$, J_{P-C} = 6 Hz) 64.4, (d, *C*H$_2$, J_{P-C} = 6 Hz), 16.0 (d, *C*H$_3$, J_{P-C} = 7 Hz). ^{31}P NMR ($CDCl_3$): δ −0.29. Mass spectrum (EI): *m*/*z* = 273 M$^+$).

(48) Coucouvanis, D.; Toupadakis, A.; Koo, S.-M.; Hadjikyriacou, A. *Polyhedron* **1989**, *8*, 1705.

(49) Brown, G. F.; Stiefel, E. I. *J. Chem. Soc., Chem. Commun.* **1970**, 728.

Table 2. UV−Visible Data for Complexes **2-15** Recorded in CH_2Cl_2

		$\lambda_{max}(\epsilon)$	
complex	R, R′	(neutral)	(protonated)
7 and **2**	quin, H	320 (10 900)	323 (5500)
		492 (5280)	378 (7830)
			648 (12 700)
8 and **3**	quin, Me	321 (14800)	325 (11 100)
		538 (3770)	389 (9660)
			729 (6400)
9 and **4**	2-pyridine, H	380 (5750)	376 (3810)
		528 (1460)	525 (6170)
10 and **5**	3-pyridine, H	371 (5540)	392 (5660)
		547 (1460)	457 (3930)
			547 sh (3250)
11 and **6**	4-pyridine, H	382 (5350)	329 (9540)
		537 (1520)	538 (8550)
12	phenyl, phenyl	371 (5030)	
		570 (1940)	
13	phenyl, H	361 (4470)	
		565 (1310)	
14	*p*-Cl-phenyl, H	369 (6710)	
		556 (1520)	
15	pyrene, H	345 (19 500)	
		351 (20 700)	
		445 (4120)	

but shifted to higher energy at a given solvent polarity. Plots of energy vs E^*_{MLCT} are commonly grouped by solvent family, and these observations are generally attributed to association of certain solvents with the molecule in question.[44] The transition is not particularly sensitive to R group substitution, and a subtle change such as replacing a *p*-H with a *p*-Cl in **13** and **14**, respectively, is barely discernible. Given the solvent sensitivity as well as the assignment of a similar transition in other Cp_2Mo sulfur ligated complexes,[50] this transition has been assigned to a weak 1,2-enedithiolate to metal charge transfer transition (LMCT). The lack of sensitivity to R-group changes on the 1,2-enedithiolate suggests that the donor orbital is localized on the 1,2-enedithiolate and interacts poorly with appended groups. This is consistent with a metallo-1,2-enedithiolate orbital that is localized primarily on the sulfur atoms. The acceptor orbital is thought to be primarily the metal d(*xz*) orbital.[50]

Additional low energy electronic transition are observed with the strongest bands found at 360−380 nm in the pyridine- and phenyl-containing complexes, **9**−**13**, at 445 nm in the pyrene complex **15**, and at 492 and 538 nm in the quinoxaline complexes **7** and **8**. This transition is sensitive to the substitution of the 1,2-enedithiolate as is evident by the ≈1740 cm^{-1} red shift upon replacing the H in **7** with Me in **8**. The red shift upon methyl substitution rules out assignment of this transition to a MLCT. In complexes **7**−**11**, all containing a basic nitrogen, the absorbance is substantially red shifted upon protonation of the heterocycle. A lack of such a red shift upon the addition of acid to complexes **12**−**15**, supports protonation occurring at the heterocyclic nitrogen in **7**−**11**. The red shift upon protonation is least pronounced in the 3-pyridine-containing complex where it is ≈1450 cm^{-1}, as shown in Figure 5. Protonation of the 2-pyridine- and 4-pyridine-containing complexes results in red shifts of 7270 cm^{-1} (380 to 525 nm) and 7590 cm^{-1} (382 to 538 nm), respectively. These shifts are accompanied by an increase in the extinction coefficient that results in an overshadowing of the LMCT band in **4** and **6**. With a small red shift upon protonation of the 3-pyridine-containing complex, the lowest energy band in complex **5** is still the LMCT, which is clearly visible in Figure 5, insert B.

(50) Bruce, A. E.; Bruce, M. R. M.; Sclafani, A.; Tyler, D. R. *Organometallics* **1984**, *3*, 1610.

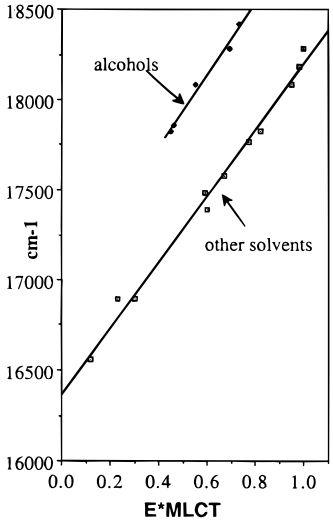

Figure 4. Plots of absorbance energy vs E^*_{MLCT} for complex **12**.

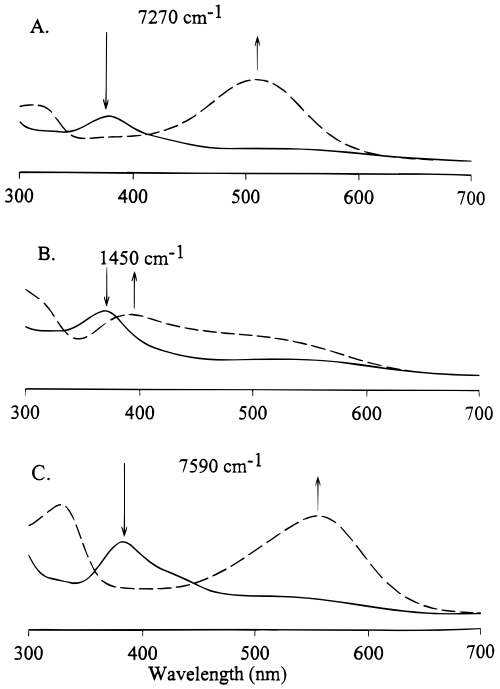

Figure 5. UV−vis absorption spectra: (a) **9** → **4**; (b) **10** → **5**; (c) **11** → **6**. The arrows ↓ denote the position of the acid-sensitive ILCT band in the neutral complexes. The arrows ↑ denote the position of the acid-sensitive ILCT band in the protonated complexes. The values shown are the energy differences between this transition in the neutral and protonated complexes.

Protonation of the 2-quinoxaline complexes **7** and **8** also red shifts this absorbance by 4890 cm^{-1} (492 to 648 nm) and 4870 cm^{-1} (538 to 729 nm), respectively. Methyl substitution of the 1,2-enedithiolate again red shifts the transition (≈1715 cm^{-1}). As stated above, methyl substitution of the 1,2-enedithiolate in the neutral complexes red shifts the transition by ≈ 1740 cm^{-1}. The similarity in the red shifts of the absorbances upon methyl substitution suggests a common origin for the lowest energy bands in the neutral and protonated complexes. The red shift upon protonation and further red shift upon methyl substitution rules out assignment of this band to either a d → d, a MLCT, or a LMCT transition.

The acid-sensitive transition of **7** shifts to lower energy in more polar solvents. This bathochromic shift with increasing polarity is the opposite of what is observed for the LMCT transition. In the protonated complex **2**, the acid-sensitive

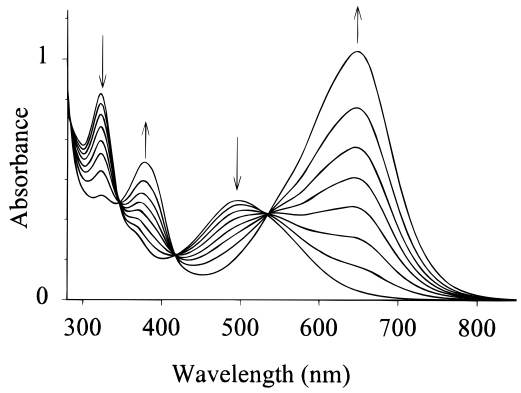

Figure 6. Titration of **7** with HBF_4 to generate **2** as monitored by UV−visible spectroscopy. The arrows ↓ denote the absorbances decreasing upon the addition of acid. The arrows ↑ denote the absorbances increasing upon the addition of acid.

transitions shifts to higher energy in more polar solvents. While the energy of the acid-sensitive transitions is effected by solvent, attempts to rectify these energy shifts with the polarity constants E^*_{MLCT} and π^* for 15 solvents gave rather poor fits to a single line. The graphs vs π^* gave marginally better fits than those vs E^*_{MLCT}.[44] Plots of energy vs either E^*_{MLCT} and π^* for just the chlorinated solvents or the alcohols did not improve the correlations.

The assignment most consistent with the red shift upon heterocycle protonation, continued red shift upon methyl substitution of the 1,2-enedithiolate, and the solvent sensitivity is an intraligand charge transfer transition (ILCT). The donor orbital is thought to be on the 1,2-enedithiolate, and the acceptor orbital is near the site of protonation. This is best described as a 1,2-enedithiolate $\pi \rightarrow$ aromatic π^* charge transfer transition. Since neither E^*_{MLCT} or π^* were derived for an ILCT transition, it is not surprizing that the energy shifts observed with solvent polarity were not modeled by either of these polarity constants.

Further support for this assignment comes from related work on a similar family of complexes (dppe)M{η^2-SC(2-quinoxaline)C(R)S} (M = Ni, Pd, Pt; R = H, Me).[11] These complexes contain acid-sensitive electronic transitions similar to those of **7** and **8**. These transitions are nearly equivalent for the corresponding Ni, Pd, and Pt complexes (differing by ≤5 nm). It is expected that if these transitions had considerable MLCT (or LMCT) character, they would be substantially more sensitive to the metal center.[51−55] While plots of the absorption energy vs either E^*_{MLCT} and π^* for **7** were not linear, a plot of the absorption energies of **7** vs the absorption energies of (dppe)-Pd{η^2-SC(2-quinoxaline)C(R)S}in a given solvent was linear. This suggests that this absorbance can be assigned to the same electronic transition in both the group VI and group VIII metal complexes and supports the ligand nature of this transition.

The relatively small energy shift of the ILCT upon protonation in the 3-pyridine complex, **10**, relative to the 2- or 4-pyridine complexes, **9** and **11**, is expected given the resonance structures shown for the pyridine complexes in eqs 9 and 10.[13] The 1,2-enedithiolate ligand stabilizes the protonated 2- and 4-substituted heterocycles through resonance forms B and C. As will be discussed, this also has a profound effect on the pK_a of the 2- and 4-substituted heterocycles.

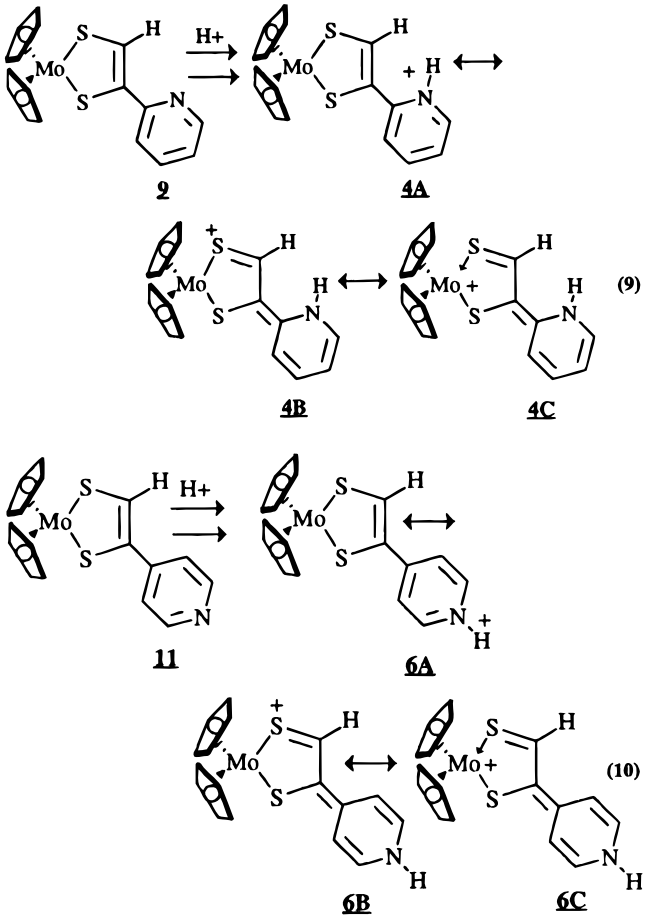

The 3-pyridine complex **5** only has resonance form A available. Protonation of the 3-pyridine complex (**10** → **5**) will lower the π^* orbital of the heterocycle but will have little affect upon the donating 1,2-enedithiolate π orbital. This results in a relatively small energy shift of the ILCT band upon protonation. Not only does protonation of the 2- and 4-substituted complexes lower the π^* orbital of the heterocycle, but resonance forms B and C would raise the energy of the 1,2-enedithiolate π orbital, thereby, adding to the red shift of the ILCT band upon protonation.

As shown for the conversion of **7** → **2**, in Figure 6, protonation appears to be a clean reaction; however, a trace paramagnetic impurity is generated. The paramagnetic impurity accounts for less than 5% of the sample as measured by ESR against a Mo^V standard. Addition of base eliminated the presence of the Mo^V complex and converts the protonated complexes to their neutral analogs. The identity of this Mo^V complex has yet to be determined.

The addition of excess HBF_4 to the quinoxaline complexes **2** and **3** in nonpolar solvents leads to an additional red shift (≈2300 cm^{-1}) of the band assigned to the ILCT transition. This has been assigned to a second protonation of the quinoxaline ligand and the formation of a dicationic complex. These complexes are extremely acidic and readily lose the second proton in the presence of even weakly basic substrates, reverting to the monoprotonated species.

^{1}H NMR and IR. In the ^{1}H NMR all of the neutral complexes have cyclopentadienyl resonances at 5.3 (±0.05) ppm. The protonation of **7**−**11** results in downfield shifts of ≈ 0.1 ppm for the cyclopentadienyl resonances, while the other resonances associated with **2**−**6** are shifted downfield by between 0.2 and 0.3 ppm. The resonances of the protonated complexes are broadened slightly, presumably due to the Mo^V impurity.

(51) Gray, H. B.; Ballhausen, C. J. *J. Am. Chem. Soc.* **1963**, *85*, 260.
(52) Shupack, S. I.; Billig, E. C.; Williams, R.; Gray, H. B. *J. Am. Chem. Soc.* **1964**, *86*, 4594.
(53) Werden, B. G.; Billig, E.; Gray, H. B. *Inorg. Chem.* **1966**, *5*, 78.
(54) Fackler, J. P.; Coucouvanis, D. J. *J. Am. Chem. Soc.* **1966**, *88*, 3913.
(55) Bowmaker, G. A.; Boyd, P. D. W.; Campbell, G. K. *Inorg. Chem.* **1983**, *22*, 1208.

Table 3. pK_a Values for Complexes **2**−**6** in Acetonitrile

complex	R, R′	pK_a
2	2-quinoxaline, H	12.1 ± 0.1
3	2-quinoxaline, Me	11.1 ± 0.1
4	2-pyridine, H	15.4 ± 0.2
5	3-pyridine, H	13.5 ± 0.2
6	4-pyridine, H	15.2 ± 0.1

In addition to infrared bands associated with the cyclopentadienyl groups, complexes **7**−**11** have bands associated with the C═N and C═C stretching modes of the heterocycles and 1,2-enedithiolate. In the quinoxaline containing complex **7**, two of these bands, at 1540 and 1505 cm^{-1}, shift to 1595 and 1574 cm^{-1} upon protonation. Protonation of the pyridine complexes, however, led to only subtle changes in the energy of these stretching modes ($\leq$10 cm^{-1}).

The C═C and M−S stretching modes of the 1,2-enedithiolate are difficult to properly assign. These bands have only been reliable assigned in a small number of 1,2-enedithiolate complexes using linear coordinate analysis.[56−59] Attempts to identify the N−H^+ stretching modes in the protonated complexes were obscured by C−H stretching bands at $\approx$3000 cm^{-1}.

pK_a Measurements. In an attempt to better understand the fundamental properties of heterocyclic substituted metallo-1,2-enedithiolates, the pK_a values for **2**−**6** were measured. The pK_a measurements where made in accord with the equilibrium shown in eq 11, using [pyridinium][BPh_4] (pK_a = 12.3 acetonitrile)[45]

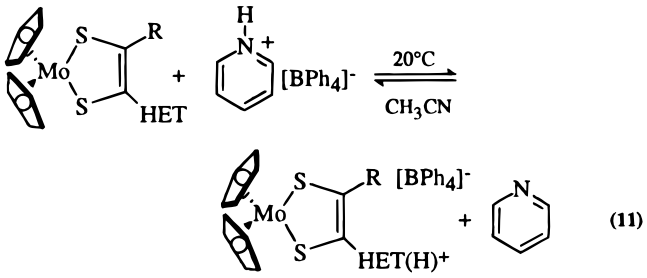

as the acid. The reactions were easily followed by UV−visible spectroscopy and a summary of the results are shown in Table 3. In acetonitrile the pK_a values for the pyridine-containing metal complexes are 1−3 units higher than that of pyridinium. The pK_a value for quinoxalinium is not known in acetonitrile, but from the aqueous value and the observed pK_a shifts in CH_3CN of other aromatic heterocycles, it is assumed that the values would be in the 9−10 range. As such, the quinoxaline complexes, like their pyridine analogs, are more basic than the free heterocycle by 2−3 pK_a units.

The pK_a values for the substituted pyridinium complexes follows the pyridine substitution trend 2 $\approx$ 4 > 3 > free pyridinium. The increase in the pK_a of all the pyridines along with the pyridine trend is consistent with resonance stabilization of the protonated heterocycle by the 1,2-enedithiolate. As shown in eqs 9 and 10, resonance forms **B** and **C** localize the positive charge on the 1,2-enedithiolate and the metal center, respectively. The absence of this resonance stabilization in **5** accounts for the relatively lower pK_a of this complex.

The increase in the pK_a of **4**−**6** relative to the parent heterocycle is similar to that of 2-, 3-, and 4-aminopyridiniums.

Table 4. $E_{1/2}$ Values for Complexes **7**−**15**[a]

complex	R R′	$E_{1/2}$ (mV)
7	2-quinoxaline (H)	256
8	2-quinoxaline (Me)	200
9	2-pyridine (H)	173
10	3-pyridine (H)	200
11	4-pyridine (H)	171
12	phenyl (phenyl)	118
13	phenyl (H)	119
14	p-Cl-phenyl (H)	158
15	pyrene (H)	121

[a] The values are reported in CH_2Cl_2 vs Ag/AgCl where the ferrocene/ferrocenium is found at 452 mV.

These findings suggest that the metallo-1,2-enedithiolate is as good at resonance stabilizing pyridinium as an amino functional group.

Resonance forms **A**, **B**, and **C** are also available to the 2-quinoxalinium complexes, assuming protonation of N(1), as shown in eq 12. This accounts for the increase in basicity of

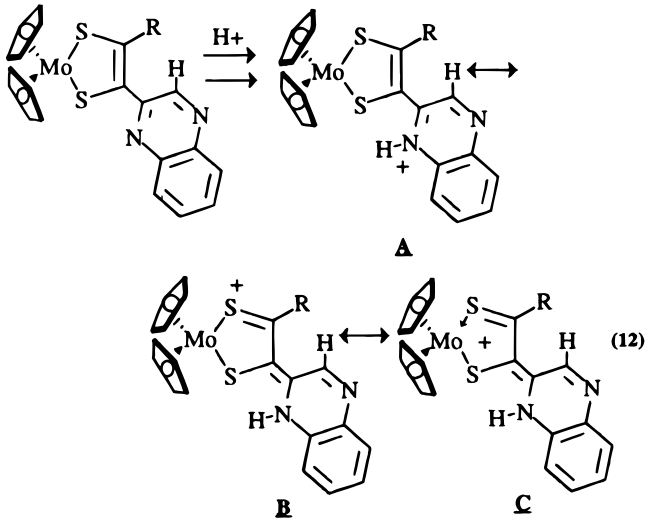

the quinoxalines in **7** and **8** relative to the parent heterocycle. The pK_a value for **2** is close to that predicted for 2-aminoquinoxaline assuming an eight unit shift in acetonitrile from the value in H_2O. The more electron rich **8**, however, is less basic than complex **7**. The pK_a drop suggests that resonance forms **B** and **C** are less important in the methyl-substituted complex. In these resonance forms, maximum conjugation occurs when the 1,2-enedithiolate is coplanar with the protonated heterocycle. The methyl group would be expected to hinder this coplanarity, decreasing the importance of these resonance forms and lower the pK_a of **3** relative to **2**.

Electrochemistry. As shown in Table 4 (see Figure 7), all of the complexes prepared in this study possess reversible Mo^{IV}/Mo^{V} oxidation waves. The $E_{1/2}$ values are sensitive to the R-groups as expected. Replacing a *p*-H with a *p*-Cl shifts the $E_{1/2}$ value by $\approx$40 mV, making **14** more difficult to oxidize than **13** and methyl substitution of the 1,2-enedithiolate makes complex **8** easier to oxidize than **7** by 56 mV. While the Mo^{V} species where stable on the electrochemical time scale, a stable Mo^{V} ESR signal was not observed in attempts to prepare these complexes by chemical oxidation.

Protonation of complexes **7**−**11** shifts the reversible Mo^{IV}/Mo^{V} redox potentials to more positive values as expected. The $E_{1/2}$ for complexes that do not possess an appended basic site are shifted $\leq$10 mV upon the addition of acid. The redox potential shifts $\Delta E_{1/2}$ {$\Delta E_{1/2} = E_{1/2(\text{protonated})} - E_{1/2(\text{neutral})}$} for **7**−**11** are dependent upon the acid used. In general, a stronger

(56) Kilpatrick, L.; Rajagopalan, K. V.; Hilton, J.; Bastian, N. R.; Stiefel, E. I.; Pilato, R. S.; Spiro, T. G. *Biochemistry* **1995**, *34*, 3032.
(57) Subramanian, P.; Burgmayer, S.; Richards, S.; Szalai, V.; Spiro, T. G. *Inorg. Chem.* **1990**, *29*, 3849.
(58) Clark, R. J. H; Turtle, P. C. *J. Chem. Soc., Dalton Trans.* **1978**, 1714.
(59) Schlapfer, C. W.; Nakamota, K. *Inorg. Chem.* **1975**, *14*, 1338.

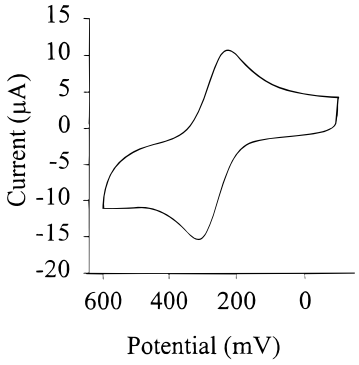

Figure 7. Cyclic voltammogram of complex **7** in CH_2Cl_2, with $[NBu_4][PF_6]$ as the supporting electrolyte. Sweep rate = 100 mV/s. The ferrocene/ferrocenium couple is found at 452 mV but is not shown.

acid results in a larger $\Delta E_{1/2}$. The positive shifts are small, ≤25 mV, for complexes **7**, **8**, and **10** when pyridinium is used as the proton source. The addition of 1 equiv of pyridinium to complexes **9** and **11** shift the potentials by ≈180 mV. The $\Delta E_{1/2}$ values, generated using pyridinium, reflect the pK_a's of the Mo^V protonated complexes more than the $E_{1/2}$ values for the protonated species. The protonated Mo^V species are expected to be more acidic than the corresponding Mo^{IV} complexes and would readily loss a proton (to pyridine) once generated under conditions where the protonated Mo^{IV} complexes are the dominate species in solution. This results in relatively small changes in the $E_{1/2}$ values that roughly follow the pK_a trend established for the Mo^{IV} complexes.

When excess HBF_4−etherate is used to protonate complexes **7**−**11**, the $\Delta E_{1/2}$ values are much larger. The $\Delta E_{1/2}$ values for complexes **7**−**9** are between 200 and 220 mV, while for complex **10** and **11** they are 375 and 310 mV, respectively. These values are consistent with those obtained using the isolated complexes.

Conclusion

This work demostrates that α-substituted ketones are ideal starting materials for the synthesis of metallo-1,2-enedithiolates. Metallo bis(hydrosulfido) complexes, such as $Cp_2Mo(SH)_2$, directly convert α-bromo, α-tosyl, and α-phosphorylated ketones to metallo-1,2-enedithiolates. The Cp_2Mo complexes are easily prepared from convenient air stable metallic and organic starting materials, and this method is amenable to a broad range of functional groups. While this paper reports the synthesis of complexes of Cp_2Mo, future reports will include studies of the group VIII metal hydrosulfido complexes,[11] as well as reactions of the thiomolybdates with similar organic substrates. All of these reactions lead to the formation of metallo-1,2-enedithiolates.

The complexes prepared in this study have allowed the general properties of heterocyclic substituted metallo-1,2-enedithiolates to be explored. While it is expected that d^2 metallo-1,2-enedithiolates possess a LMCT transition, the heterocyclic-substituted complexes prepared in this study have an additional transition with energies that are extremely acid sensitive. This transition has been assigned to an intraligand charge transfer transition (ILCT), that is 1,2-enedithiolate $\pi \rightarrow$ aromatic π^* in character.

It has also been demonstrated that the 1,2-enedithiolate ligand when appended to a heterocycle greatly affects the chemistry of the heterocycle. In particular, a metallo-1,2-enedithiolate can increases the basicity of an appended aromatic heterocycles by as much as 3 pK_a units through resonance stabilization of the protonated species. This increase is equivalent to that imposed by a similar amino group substitution.

Acknowledgment. We are indebted to the American Chemical Society, Petroleum Research Fund (Grant No. 28499-G3) and the American Heart Association, Maryland Chapter (Grant No. MDBG0695) for funding We are also indebted to the National Science Foundation for an REU grant. (Grant No. CHE-9300336) for the support of C.J.B. in the summer of 1994.

Supporting Information Available: Tables listing details crystallographic data, positional parameters, anisotropic thermal parameters, and bond lengths and angles, (18 pages). Ordering information is given on any current masthead page.

IC9602052